Horizontal Bloch lines and anisotropic-dark-field observations

Karel Patek,* André Thiaville, and Jacques Miltat
Laboratoire de Physique des Solides, Bâtiment 510, Université Paris–Sud and Centre National de la Recherche Scientifique, 91405 Orsay Cedex, France

(Received 3 May 1993; revised manuscript received 19 October 1993)

Anisotropic-dark-field optical imaging is shown to reveal the presence of horizontal Bloch lines (HBL's) in the moving walls of bubble garnets. It relies on the deformation of the wall shape under dynamic conditions due to the presence of a HBL. The wall tilt is detected because it affects the intensity of the wall images much in the same way as localized wall tilts reveal the location of vertical Bloch lines (VBL's) in static conditions. Quantitative time-resolved measurements of wall intensity are presented and shown to compare very favorably with numerical computations. These use a simplified spin dynamics equation (Slonczewski's equations) describing the wall position and wall-core magnetization in-plane angle, as a function of position across the thickness, and time. Dynamic reversals of VBL's contrast have also been observed. The fact that they occur for one half of the possible configurations is puzzling. They are tentatively explained on the basis of a dynamically induced charge distribution at VBL location, which arises from a wall wave developing around the moving VBL.

I. INTRODUCTION

The knowledge of the behavior at a microscopic scale, namely the domains scale, of a magnetic material, is a prerequisite to the understanding of its macroscopic properties. Moreover, as meaningfully demonstrated during the development of bubble memories, the properties of domains are themselves strongly dependent on the structure of the walls limiting them.[1] In fact, a domain wall can sustain different magnetization orientations at its core, separated by (Bloch) lines. In the bubble terminology,[1] which applies to a thin film with perpendicular easy axis, a distinction is made according to the orientation of the line. Vertical lines (running parallel to the easy axis) and horizontal lines are the extreme cases [vertical Bloch lines (VBL) and horizontal Bloch lines (HBL), respectively, in the following, see Fig. 1(a)].

The former are stable structures of finite length, the sample thickness. A memory scheme using a stable pair of VBL as information bit is presently under study following the original proposal of Konishi.[2] The story of VBL's observation is quite instructive. Lorentz microscopy provided direct evidence of their existence in bubble materials.[3] Then, together with a vastly improved knowledge of the dynamic properties of walls and lines, dynamic optical techniques were devised,[4–6,2] according to which VBL's are detected by a flexure of the wall linked to a reduction of the wall transient displacement at line position. More recently, a method for the static optical observation of VBL's was discovered. It uses light diffraction by the domain wall in an anisotropic-dark-field arrangement. That technique relies on a local wall deformation, namely a tilt away from the film's normal, which occurs in order to reduce the magnetostatic energy of the line.[7] Indeed, as displayed schematically in Fig. 1(b), magnetostatic charges (the so-called σ charges,[1] equal to $\mathrm{div}_{\parallel}\mathbf{m}=\partial m_x/\partial x+\partial m_z/\partial z$; $\mathbf{m}=\mathbf{M}/M_s$, $\mathbf{M}$: magnetization vector) arise at a VBL due to the wall magnetization distribution. Furthermore, experiments on VBL's demonstrated the high sensitivity of the anisotropic-dark-field mode to wall tilts.

Horizontal lines are nonstable in zero field, and of arbitrary length determined only by the experimental conditions. They thus prove quite difficult to observe, in principle. On the other hand, they are intimately bound to

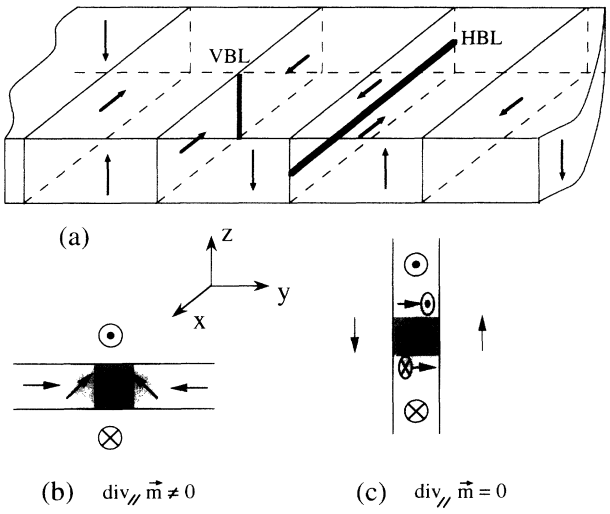

FIG. 1. (a) General drawing of domains, walls (shaded) and lines in a bubble garnet film, in which the easy axis is perpendicular to the film plane. The coordinate system used throughout the paper is figured, with z the easy axis, y the wall normal, and x along the wall. The magnetization distributions characteristic of a vertical Bloch line (VBL) and a horizontal Bloch line (HBL) are shown in (b) (view along z axis) and (c) (view along x axis), respectively. The magnetization direction $\mathbf{m}$ is symbolized by arrows when in the drawing plane and by dot (resp. cross) when perpendicular to that plane, pointing toward (resp. away from) the observer.

0163-1829/94/49(10)/6678(11)/$06.00

the transient states in a wall under dynamic structure transformation.[1] HBL's, therefore, are objects of prime importance for wall dynamics in bubble garnets. The experimental techniques already quoted for VBL's,[4,5] revealed when applied to HBL's, that the latter were also affecting wall motion.[5,8] A more direct measurement of HBL motion would, however, be valuable as a test of the current wall dynamics models. Coming back to the anisotropic-dark-field technique, no contrast is expected from HBL's, because, as demonstrated schematically in Fig. 1(c), their magnetic microstructure in the wall is charge free in opposition to the VBL case: The wall does not need to tilt at the HBL location. On the other hand, now in similarity with the VBL case, a moving wall is anticipated to wrap somehow around the HBL: This will affect the wall geometry. It was thus to be expected that the influence of HBL's on wall geometry could result in a wall tilt detectable by means of anisotropic-dark-field optical microscopy.

Experiments were undertaken along these lines of thought, and indeed changes in wall brightness were observed. Just to provide a proof of this statement, and give a flavor of the phenomena discussed in this work, it has been felt useful to exhibit Fig. 2 at this stage. A set of nearly parallel walls is observed in anisotropic dark field, some of them containing VBL's which are marked by arrows. The pictures were taken with the walls at rest 2(a), then moving [2(b) and 2(c)]. It can be seen that the walls brightnesses change, becoming brighter or darker in 2(b) and vice versa in 2(c). The contrast evolutions of wall segments separated by a VBL are opposite. Finally one VBL image is seen to change contrast.

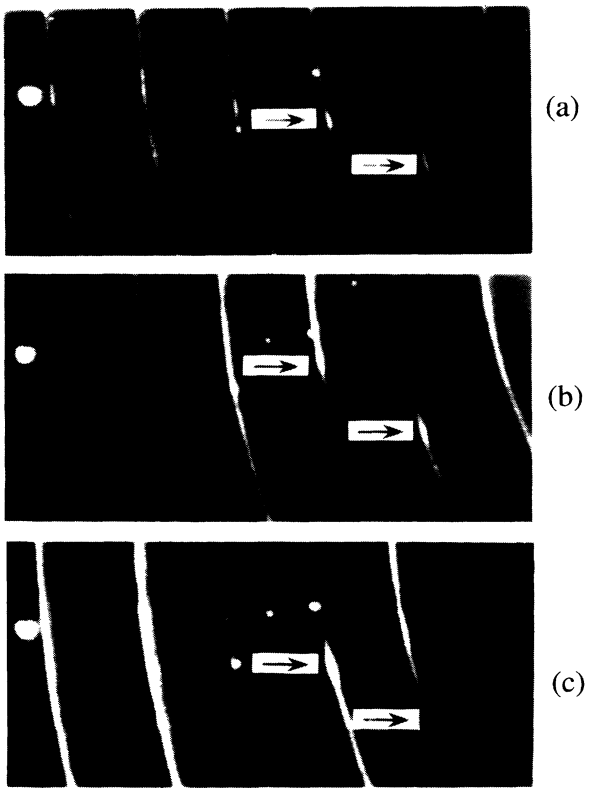

FIG. 2. Effect of a 10 Oe, 500 ns duration z-field pulse on the sample, as revealed by anisotropic-dark-field observation. (a) Wall picture at rest. Arrows indicate the location of VBL's. The other pictures are taken at a time t after pulse onset, with $t=35$ ns for (b) and $t=60$ ns for (c). Field of view: $65\times30\ \mu m^2$.

In the rest of the paper, these phenomena will be quantitatively studied. Section II describes the experimental setup and sample, and presents the anisotropic-dark-field observation technique. Section III shows experimental results for the case of a wall without VBL, and their interpretation by means of increasingly complex models. Section IV focuses on the time evolution of wall contrast at a VBL and discusses it.

Before closing this introduction, let us mention that this work has partially been presented during the 6th Workshop dedicated to VBL memories[9] and that observations similar to those of Fig. 2 have been performed independently by Nicolaev and Logginov.[10]

II. EXPERIMENTAL DETAILS

A. Optical technique

The key technique which enables these experiments being the observation in anisotropic dark field, its principle and physical interpretation will be exposed first.

In a general dark-field image, uniform parts of the object appear dark, and, e.g., particles which scatter light are seen as bright spots. For a magnetic sample having domains much larger than the wavelength of light, these domains are uniform and, therefore, appear dark. At the domain wall, due to the magneto-optical effect, the refractive index is a steplike function and all points on the wall will scatter light. Collecting the coherently scattered amplitudes by all locations on the wall amounts to a diffraction calculation, which bears some resemblance with the diffraction of x rays by atoms in a crystal. The usual dark field is realized by inserting a stop with an annular hole (with an aperture larger than the numerical aperture of the objective) in the aperture plane of the microscope condenser, and may be called isotropic. Reducing the hole to a small part of the ring removes the rotation symmetry around the microscope axis. Now the incident light has an average wave vector $\mathbf{K}$ with a nonzero in-plane projection denoted by $\mathbf{k}$. In the present setup, shown in general view on Fig. 3, $\mathbf{k}$ lies along the y axis. Requirements for anisotropic-dark-field observation are now met.

The well known example of diffraction by a slit indicates that walls perpendicular to $\mathbf{k}$, i.e., along the x axis, will diffract light most. The experimental arrangement complies with this geometry. In the following, the term contrast (against the dark domains) will refer to the intensity diffracted by an object, such as wall or line.

Experimental work (for example, Refs. 7 and 11) has progressively shown that the magnetization inside the wall is not directly sensed, but that the wall shape is relevant. The simplest nontrivial shape is a tilt, away from the z direction. In order to explain why a tilt affects the diffracted intensity, let it be recalled that the total diffracted amplitude is the sum of the complex exponentials of the phase differences between the incident and

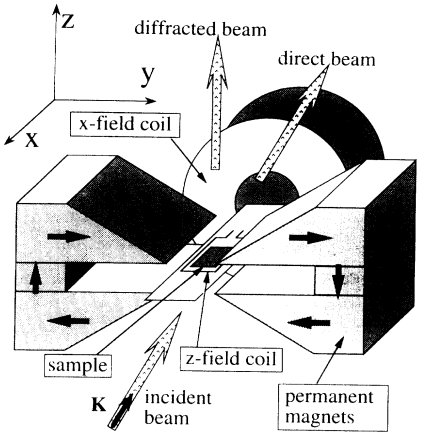

FIG. 3. Z-field gradient setup with drive coils. The incident, direct and diffracted optical beams are also drawn. **K** is the wave vector of the incident light, **k** its projection onto the sample plane, and lies along the y axis.

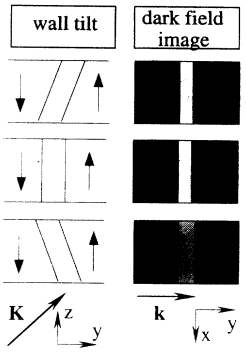

FIG. 4. Schematic relation between wall tilt and contrast under anisotropic-dark-field illumination.

diffracted waves on all scattering centers. If that phase difference does not vary appreciably over the diffracting object, the scatterers are well in phase and the total amplitude strong. Let θ_i (resp. θ_d) denote the angle of the incident (resp. diffracted) beam in the sample, measured from the z axis, and β the tilt angle. The variation of the phase difference between the two endpoints of the wall (on the surfaces of the film) reads straightforwardly

$$\Delta\Psi(\beta)=(2n\pi h/\lambda)[(\cos\theta_d-\cos\theta_i)+(\sin\theta_d-\sin\theta_i)\tan\beta] \quad (1)$$

with n being the refractive index and λ the wavelength of light. When compared to a vertical wall, one direction of tilt reduces, and the other increases, $\Delta\Psi$. In the isotropic-dark-field mode, beams with opposite θ's would cancel, thus removing the sensitivity to the sign of β. In the following, parameters do amount to $n=2.2$, $\lambda=0.59$ μm, $n\cdot\sin\theta_i=0.6$, $n\cdot\sin\theta_d=0.35$ (the experimental values). Equation (1) now reads

$$\Delta\Psi(\beta)=2\pi[0.54-2.42\tan\beta] \quad (2)$$

indicating that a small tilt (e.g., 1 degree) non-negligibly affects $\Delta\Psi$. Since, for a tilted but still planar wall, the wall intensity reads

$$I(\beta)\propto[\sin(\Delta\Psi/2)/(\Delta\Psi/2)]^2 \quad (3)$$

one obtains $I(\beta=3\text{ degrees})=1.6I(\beta=0)$; $I(\beta=-3\text{ degrees})=0.5I(\beta=0)$, i.e., quantities typical of the experimentally measured values.

Thus, simply stated, a tilt such that the wall becomes more (resp. less) inclined with respect to **K** will give rise to a diffracted intensity smaller (resp. larger) than that of the vertical wall (Fig. 4). Thus follows the rule which is the basis of our qualitative interpretation of the wall contrast time evolution. Expansion of the above results to a nonplanar wall yields[12]

$$I=\left|\frac{\lambda}{n\pi(\sin\theta_i-\sin\theta_d)}\int_{-h/2}^{h/2}\exp\left\{i\frac{2\pi n}{\lambda}[q(z)(\sin\theta_i-\sin\theta_d)+z(\cos\theta_i-\cos\theta_d)]\right\}dz\right|^2, \quad (4)$$

where $q(z)$ denotes the depth-dependent wall position.

Looking at Fig. 4, little effort should be made to understand VBL contrast. The wall tilts in the vicinity of the VBL in order to compensate the VBL σ charge: From the sign of that charge one deduces the tilt direction and, from Fig. 4, the contrast. Of course, the amount of tilt as well as its x extension depend on the material parameters, mainly the quality factor (defined below) Q (Ref. 7).

B. Sample and apparatus

All quantitative measurements of time-resolved wall contrast have been performed under the following conditions: The sample was inserted inside a mighty magnetic z-field gradient (2.3 Oe/μm) large enough to generate a single domain wall sitting in a potential well (Fig. 3). This technique already successfully utilized for domain-wall time-response detection (e.g., Ref. 13) was initially implemented in order to study the dynamic properties of VBL's.[11,7,14] The stabilization of a single wall in the existing field gradient imposes severe limitations onto permissible material parameters.[15] Observations have therefore been limited to a single garnet material [composition $(GdTmPrBi)_3(FeGa)_5O_{12}$] with the following parameters: thickness $h=5.71$ μm, magnetization $4\pi M_s=113$ G, quality factor $Q=11.8$ (the ratio of uniaxial energy constant K_u to demagnetizing field energy $2\pi M_s^2$), characteristic length $l=1.44$ μm. The characteristic length is a ratio relating the wall and demagnetizing field energies: $l=(1/2)(\sigma_w/2\pi M_s^2)$; $\sigma_w=4(AK_u)^{1/2}$; A is the exchange constant. Dynamic parameters are the gyromagnetic ra-

tio $\gamma = 1.8 \times 10^7$ $Oe^{-1}s^{-1}$ and the damping constant $\alpha = 0.145$, estimated from the ferromagnetic resonance linewidth.[1]

Anisotropic-dark-field observations were performed on a standard microscope relying on, however, a modified dark-field condenser.[11] A continuous Hg lamp and a frequency-doubled, pulsed Nd:YAG laser with 10-ns pulse width, pumping a homemade broadband dye laser (an efficient way of removing unwanted image speckle) were used as light sources.

A six-turns rectangular (5×13 mm) coil was used to apply z-field pulses to the sample. The coil impedance did allow for a 30 ns pulse rise time. Observations with the pulsed light source were obtained in the stroboscopic mode, at the repetition frequency of the laser (20 Hz). The continuous lamp was first used to check that the pulse duration and/or amplitude were chosen such as not induce any permanent modification of the wall state, as monitored by its dark-field image before and after pulse application. Subsequently, varying the delay between the beginning of the field pulse and the light pulse did allow for the observation of the time evolution of the magnetic structure with a few nanoseconds time resolution.

Lastly, an additional coil did provide a static field along the x direction, whereas a static field along the y direction could be simply applied to the sample by means of a modification of the z position of the sample within the z-field gradient ($\partial H_z/\partial y = \partial H_y/\partial z$).

In order to relate wall contrast variations to transient wall configurations, a precise knowledge of the domain magnetization directions as well as the Bloch component of the wall magnetization are required. The domain magnetizations are defined by the z-field gradient: In all pictures, the magnetization direction is downwards (upwards) in the domain to the left (right) of the wall. The wall magnetization is deduced from the contrast of a VBL bounding the wall segment under scrutiny as a consequence of the absolute contrast rules described before.

III. TIME EVOLUTION OF WALL CONTRAST

Consider a unichiral wall section, which means in practice that VBL's are far away from, and do not during the experiment enter that section. Let now a z-field pulse be applied, causing the wall to move and its contrast to change. The pulse should last long enough to ensure that the wall reaches equilibrium under field. For this sample and the restoring force of the gradient, a duration of 500 ns proved adequate. The pulse amplitudes ranged from 6 to 10 Oe, as below 6 Oe the wall contrast changed imperceptibly, and around 10 Oe the wall structure was modified after a pulse (new VBL's appeared).

A. Experimental results

For all fields, during the initial 100 ns or so, two fairly large wall contrast modifications are observed, as shown in Fig. 5. In this precise case, the intensity diffracted by the wall decreases during the first 40 ns. It then increases with a maximum at about 70 ns after the pulse onset. At this point, the diffracted intensity clearly exceeds the intensity at rest. The diffracted intensity then decreases again, reaching the initial value at $t \approx 100$ ns.

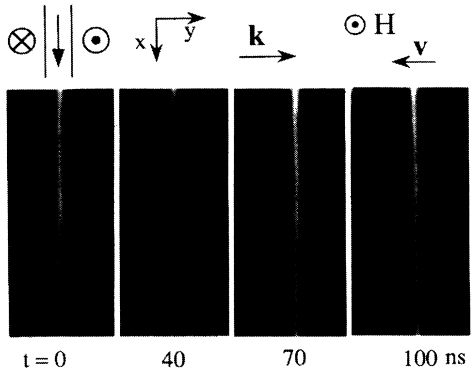

FIG. 5. Wall diffracted intensity as a function of time under the action of a 8 Oe, 500 ns duration z-field pulse. Field of view: 20×45 μm^2. The drawings refer to the experimental conditions.

In spite of a rolling averaging image treatment (we perform it over 64 frames in order to reduce the laser flash intensity fluctuations from pulse to pulse), walls whether at rest or moving exhibit a nonconstant diffracted intensity along their length. Figure 6 exhibits the variation of diffracted intensity minus background, as a function of coordinate x along the wall, corresponding to the photographs in Fig. 5. The background is the intensity measured in the domains. Although intensity fluctuations do appear non-negligible, those plots clearly put into evidence the diffracted intensity changes vs time. In order to translate the observed contrast variations into reliable figures, the diffracted intensity may now be averaged over a significant wall length, leading to intensity plots vs time such as shown in Fig. 7.

If the Bloch component of the wall magnetization is reversed, the diffracted intensity first increases, then decreases and finally increases again in the time span 0–100 ns (see Fig. 8). The latter behavior appears basically symmetrical of the former (Fig. 7) with respect to the

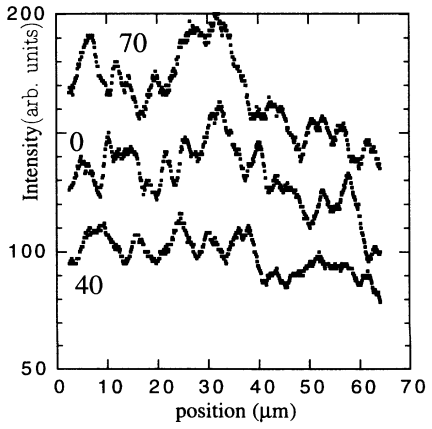

FIG. 6. Diffracted intensity minus background vs position along the wall, corresponding to the pictures at $t = 0$, 40, and 70 ns in Fig. 5.

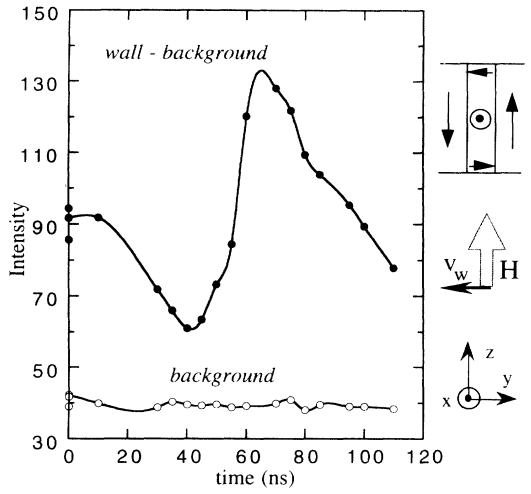

FIG. 7. Background level and diffracted intensity minus background vs time (first 100 ns) recorded for a wall with a $M_x > 0$ Bloch magnetization component. Z-field pulse amplitude 8 Oe, duration 500 ns. The curves serve as a guide to the eye.

diffracted intensity level at rest. On the contrary, if the wall velocity is reversed (by applying a negative z-field pulse), the respective intensity plots of Figs. 7 and 8 remain essentially unchanged.

At later times, as shown in Fig. 8, for example, another slower and less intense variation, of similar shape, occurs again. Then the wall has reached equilibrium under field and displays its contrast at rest.

B. Models

1. *Rigid-wall HBL model*

The simplest picture of the twisted Bloch wall dynamics is the "HBL model,"[16,17] in which one HBL forms at one surface of the film and, then, propagates. The surface at which the HBL forms changes if the wall M_x component, or the field polarity, reverses. It suffices then

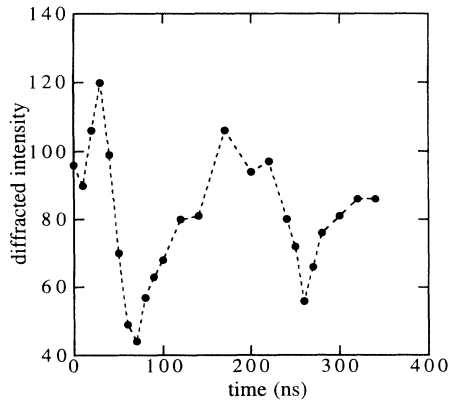

FIG. 8. Diffracted intensity minus background, recorded over the full time span, for a wall with $M_x < 0$ Bloch component. Field pulse as for Fig. 7.

to assume that the HBL slows down locally the wall to obtain a wall tilt which depends on the HBL position. Figure 9 compares experiments with these expectations, taking due care of all signs in order to determine which surface is involved each time. Drawn are the schematic tilts associated to a HBL which, at $t \approx 40$ ns, would still be located close to the surface at which it was dynamically nucleated whereas, at $t \approx 70$ ns, it would have shifted to the opposite surface. The qualitative agreement is perfect for the initial times. Therefore, the moment at which the wall contrast first returns to its rest value should be equivalent to the time at which the HBL crosses the film midplane. A quantitative comparison can be attempted. The HBL model can be solved analytically under the assumptions of a rigid wall and negligible damping, resulting in a "universal" HBL motion given by [Eq. (20) in Ref. 18]:

$$f(z_L/h) = \gamma H_z t \ , \tag{5}$$

where z_L is the HBL position in the sample thickness and f a function. Equation (5) expresses the HBL motion as due to spin precession around the total field, taken here as the applied field because the wall moves just a little during the first tens of ns. From a numerical evaluation of f, Fig. 10 follows. It indicates that the time required for a nucleated HBL to travel across half the sample thickness is $\gamma H_z t = 0.836$, which leads to the following

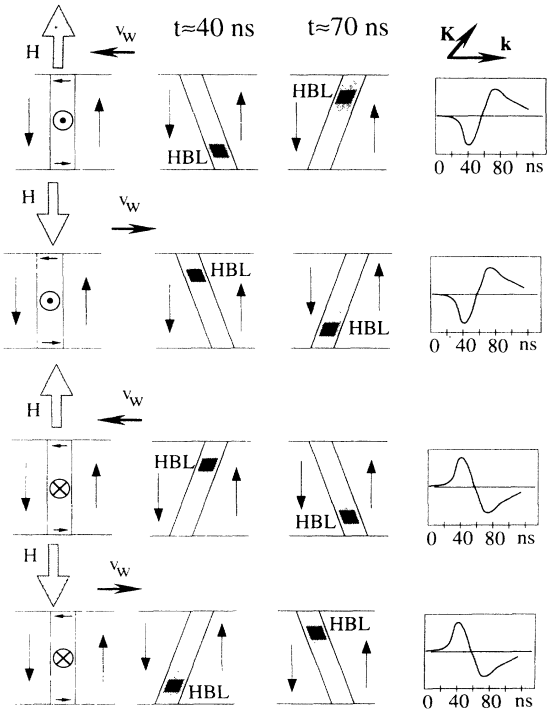

FIG. 9. Schematic time-resolved correlations between wall tilt and HBL location as a function of wall translation direction and Bloch magnetization component. The columns refer, from left to right, to the experimental conditions, the expected HBL motion with associated tilts, and the schematic experimental time evolution of wall contrast.

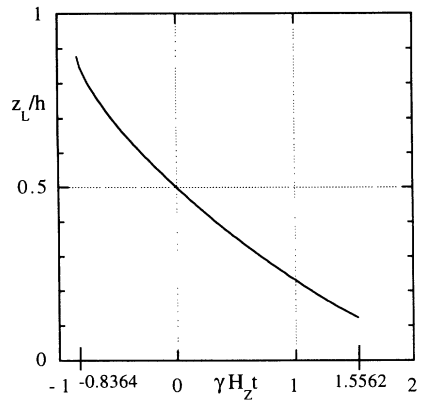

FIG. 10. Universal relation between HBL depth and reduced time in the rigid-wall model. The time $t=0$ corresponds to the HBL located at equal distances from the free surfaces.

relation:

$$t(z_L=h/2)=0.836/\gamma H_z=46.6\ \text{ns Oe}/H_z\ . \qquad (6)$$

Figure 11 shows the measured times at which two wall segments separated by a VBL first return to equal contrasts. It becomes clear that, even if a phenomenological coercive field is introduced, relation (6) grossly underestimates this time. The reason is that the model is oversimplified, as was already stressed in Ref. 18, partly because of the neglect of wall curvature.

Two behaviors are known for a HBL, after it has been nucleated.[1] First, it can reach the surface opposite to the nucleation surface and disappear there, a mechanism called punch through. The transformation of the initial wall into an opposite $\mathbf{M}_x$ wall is now complete. Then the process starts again. Second, should the total field become too low, then the HBL moves back to its original surface. Both schemes are not coherent with the measured contrast variations for $t > 100$ ns, if it is assumed that an HBL always slows down wall motion.

2. *The q-φ model*

Consequently, we resorted to a numerical procedure to solve Slonczewski's equations[17] for twisted wall motion,

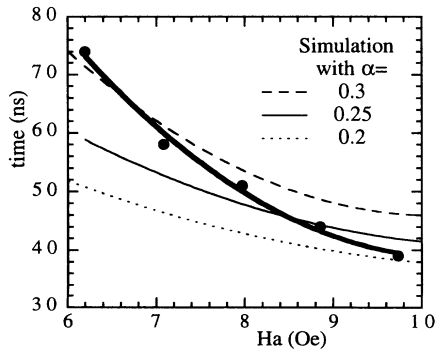

FIG. 11. Time of first return to rest value of the wall contrast, as a function of field amplitude: measured points (thick symbols and line) and calculation results for $\alpha=0.3$, 0.25, and 0.2 (q-φ model).

already used in the calculations of Ref. 18 [Eqs. (4)]. As a brief reminder, let us mention that the variables are $q(z,t)$, the wall displacement along y, and $\varphi(z,t)$, the wall magnetization in plane angle measured from the x axis. They depend on z, the position in the thickness of the film. Slonczewski's equations are two coupled nonlinear equations in these variables, derived from the Landau-Lifshitz-Gilbert equation describing the spin precession with damping, by integration across a fixed wall profile. Similarly to Ref. 18, we used a simplified evaluation of the demagnetizing field: (i) charges due to a nonvertical wall are discarded; (ii) the wall internal demagnetizing field is local (Winter approximation); (iii) a zero thickness vertical wall is assumed for the calculation of the domain stray field. The resolution procedure was adapted from Ref. 19: It uses the DPDES routine of the Fortran IMSL library, ensuring an accurate computation free of divergences (as were encountered in Ref. 18). An IBM RISC 6000 workstation solved the coupled differential equations for 1000 time steps, 1 ns each, with 200 points across the thickness, in less than 10 min. Equation (4) was then applied on the $q(z)$ profile to get the diffracted intensity, with the values of the optical parameters given in Sec. II B.

As shown in Fig. 11, a much better, although not fully perfect agreement is obtained. It was found necessary to depart from the value of α extracted from ferromagnetic resonance, in order to reproduce the results and also avoid HBL punch through, as experiments are performed with low enough fields so that this phenomenon does not occur. It is conceivable that full two-dimensional (2D) computations, which do not make the approximations specific of Slonczewski's equations, or simply a complete evaluation of the demagnetizing field, would give a better agreement. However, full 2D computations proved too demanding for the sample thickness considered, and were abandoned. Moreover, as shown below, the present relatively simple computations already provide a good agreement with experiment.

For example, Fig. 12 compares calculated values with the measured ones (identical to those of Fig. 8). The calculated intensities are just multiplied by a constant factor in order to match measurements. Focusing on the diffracted intensity, the agreement proves astonishing. A small disagreement persists about the value of the saturation wall velocity. The value $\alpha=0.25$ was chosen, but simulation results with other α's do only differ in the time scale and the peaks height, keeping the same overall shape for the contrast vs time curve. It means that the same HBL motion occurs, albeit at a different pace and with a more or less strong impact on the wall shape. It is that motion which is sensed by the diffraction of light, via the wall shape.

In order to understand more deeply the significance of the diffracted intensity curve, the figure also contains the calculated position of the HBL (defined as the position of maximum $d\varphi/dz$). Comparison of that curve with Fig. 10 shows the consequent difference in the models. This again stresses, as in Ref. 18, the necessity of allowing for wall curvature in order to compute wall dynamics realistically. For the initial times, the wall structure and shape

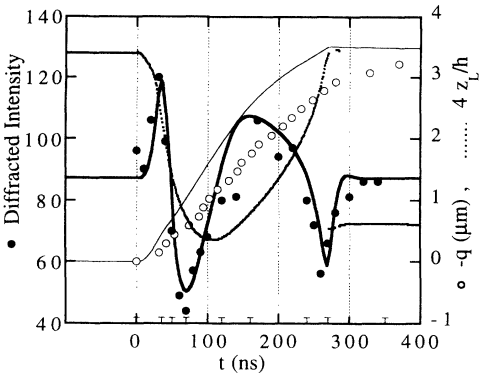

FIG. 12. Wall displacement (open symbols) and wall diffracted intensity (full symbols) measured over the full time scale of a 8 Oe, 500 ns duration z-field pulse for a wall having a $M_x < 0$ Bloch wall component. Curves are the calculated values. Also shown, by a dotted line, is the calculated HBL position, z_L/h multiplied by 4 in order to fit on the q scale. Ticks on the time axis refer to the selected times used in Fig. 13.

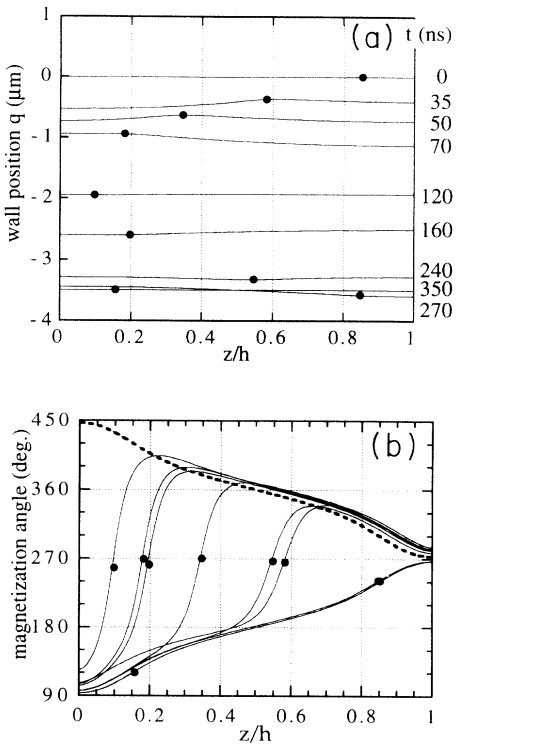

FIG. 13. Details of the calculation used for Fig. 12. Shown for selected times (contrast extrema and zero crossings) are (a) the wall profile; (b) the wall magnetization angle profile. Note that in (a) one micrometer corresponds to the same length on both axes, so that the figure indicates the true transient shape of the wall. HBL position is shown by a dot. The dashed line in (b) is the equilibrium profile for an $M_x > 0$ wall.

coincide with the corresponding drawings in Fig. 9. But, at later times, it appears that instead of causing a local lag of the wall, the HBL effect progressively turns to a local wall propulsion. We may understand that fact through energetic arguments. A HBL has a low energy at its nucleation surface, and this energy rises as the HBL translates to the other surface.[1] Therefore, as long as the HBL moves towards the other surface, energy is pumped from the field, diverted from wall propulsion, causing wall lag. Conversely, a HBL moving back to its original surface returns energy back to the wall, driving it forward locally. When the HBL disappears at its original nucleation surface, a peak in contrast whose sign is opposite to that of the peak at nucleation appears. The change of sign between these two peaks indicates opposite tilts, which correspond to opposite actions of the HBL on the wall (lag and propulsion). A subsequent minute wall oscillation can be seen, with a HBL nucleating at the other surface and disappearing there almost immediately.

Quantitatively, Fig. 13 displays z-dependent wall displacement $q(z)$ and wall magnetization angle $\varphi(z)$ profiles at some selected times indicated on Fig. 12. The HBL position is shown by a dot. Figure 13(a), at first glance, reveals just a moving planar wall containing a HBL first moving downwards, then upwards. The HBL motion is shown again in Fig. 13(b), displaying very standard curves: The HBL basically interpolates between two equilibrium wall angle profiles having $\langle\varphi\rangle = 180°$ and $\langle\varphi\rangle = 360°$, i.e., $\mathbf{M}_x < 0$ and $\mathbf{M}_x > 0$ twisted Bloch walls. A closer inspection of Fig. 13(a) reveals that, for $t < 100$ ns, the wall part close to the HBL is lagging behind the rest of the wall, by some tenths of a micrometer, whereas the converse occurs for $t > 100$ ns. That local wall propulsion, when averaged over z, is the well documented overshoot effect.[1] This effect had been measured already, on the wall displacement curves, but here shows up quite strongly in the diffracted intensity, a quantity very sensitive to wall shape. The contrast between the seemingly quiet wall displacement and the "chaotically" oscillating wall intensity stresses again the sensitivity of and the amount of information brought by small incidence angle light diffraction on the wall surface. One could parallel it to the x-ray grazing incidence diffraction method used to study the surfaces roughness at the atomic scale.

Last, a shorter (140 ns) and more intense pulse was also used. Again, a very good agreement between measured and calculated wall contrast evolution was reached.

C. Application of additional static in-plane fields

Comparison was also performed in the cases where a dc in-plane field, either along the wall (H_x) or perpendicular to it (H_y) was applied. To illustrate again the general agreement with calculations, Fig. 14 compares the effect on wall contrast of H_x [Fig. 14(a)] and H_y [Fig. 14(b)]. Sign conventions are indicated in the drawing: The x field has to be taken such as to stabilize the wall, since the other direction would soon cause the HBL to punch through.

Schematically, one can concentrate on two features of the contrast evolution, namely the time of the first zero crossing and the final peak position. Experiment and computation agree in the fact that they shift in opposite directions for H_x and in the same direction for H_y. A

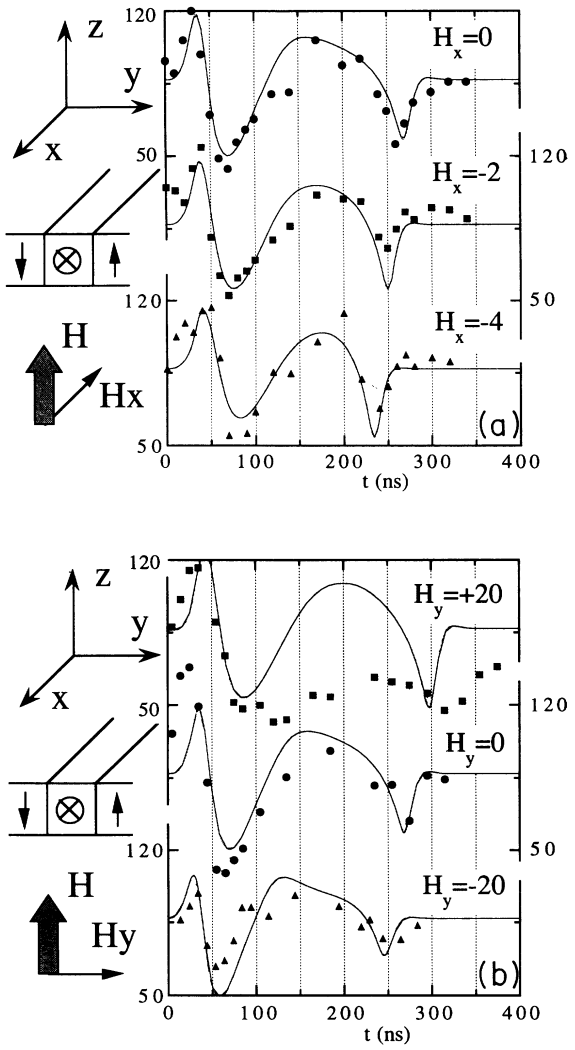

FIG. 14. In conditions identical to those of Fig. 12, influence of a static in plane field (a) parallel to the wall and along its magnetization; (b) perpendicular to the wall. Points are measurement, curves calculation. Field values are indicated in Oe. The +20 Oe values seem to suffer from an experimental artifact but still show the time shift of the salient features.

physical explanation of these effects can run as follows. The x field, lying along the wall average magnetization, applies a force which tends to restore the HBL to its original surface. Therefore, under x field, the HBL will reach the half-thickness later, and come back sooner, giving rise to time shifts in opposite directions. The influence of the y field is ten times weaker, and of a more subtle nature. The main effect here is that the two equilibrium wall angle profiles considered in Fig. 13(b) are, due to the presence of the static y field, translated in φ. For a field value of 20 Oe, calculation indicates a roughly uniform translation of the profile $\varphi(z)$ by $\approx 20°$. The two profiles prove closer for the $-y$ field, and farther apart for the $+y$ field. It follows that, in order to produce the same HBL displacement dz_L, more wall magnetization precession $d\varphi$ is necessary when $H_y = +20$ Oe than when $H_y = -20$ Oe. This means that, when compared to the zero y field case, the two contrast features considered occur both earlier for $H_y = -20$ Oe, and later when $H_y = +20$ Oe.

In conclusion of this whole section, the fair agreement found between experimental results and the theory based on Slonczewski's equation making due allowance for a distorted wall, supports the main conclusion of this paper, namely that HBL presence and position is detectable by anisotropic-dark-field optical observation. A precise picture of the processes occurring in the unichiral wall being established, we may now turn to the case of a vertical line (VBL) embedded in the wall.

IV. HBL-VBL INTERPLAY

A. Experimental evolution of wall contrast at a VBL

For a relatively long time, in fact, since our first VBL dynamic observations, we have known that, under certain circumstances, the contrast of VBL's could reverse dynamically.

Figure 15 corresponds to a winding couple of VBL's with core magnetizations as shown in the drawing. A couple is termed winding when it withstands a VBL compression by an x field, contrarily to an unwinding one.[1] The VBL contrasts [Fig. 15(a)] are opposite because their σ charges are opposite. Under a z-field pulse, the VBL's move along the wall [Fig. 15(b)] by the action of the gyrotropic force. Note that their displacement is in the same direction, as expected for a winding pair.[20] On Fig. 15(b), the reversal of VBL's contrast is apparent. But, strangely enough, the opposite pulse does not give rise to contrast reversal.

The reversal, in fact, occurs exactly in half of the cases, as is illustrated in Fig. 16: For two pulse-field polarities (causing opposite VBL displacements) there is one reversal and one nonreversal. Both field polarities exist in fact

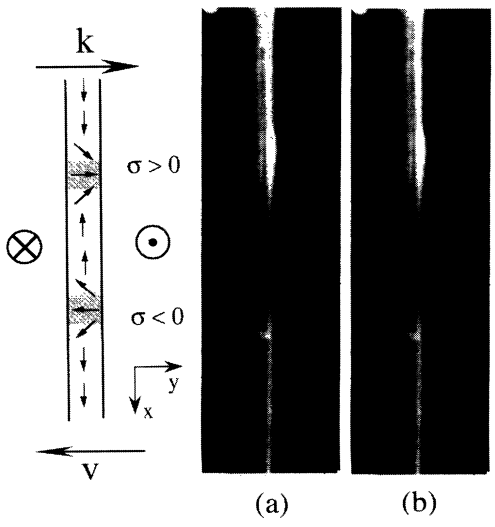

FIG. 15. A pair of winding VBL's: (a) at rest; (b) after 75 ns of a 8.8 Oe, 500 ns z-field pulse. Note the parallel displacement of both lines towards the top of the pictures and their contrast reversal between $t=0$ and $t=75$ ns. Field of view: $25 \times 85\ \mu m^2$.

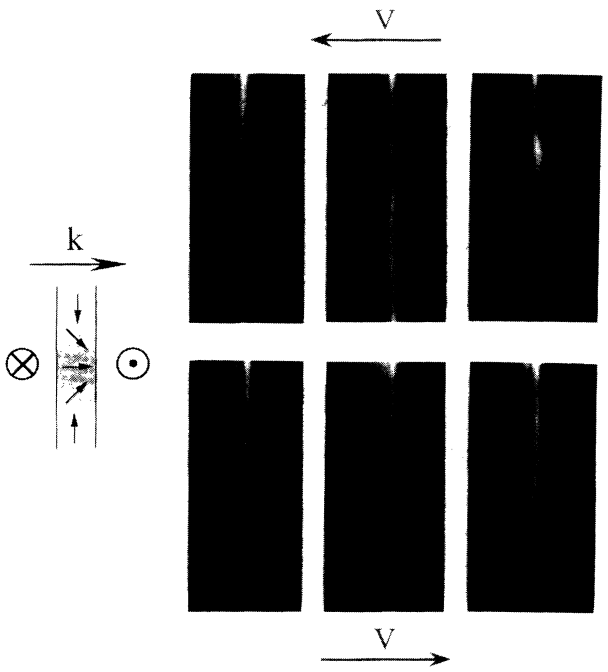

FIG. 16. Difference in dynamic VBL contrast behavior upon reversing the wall velocity: The same line undergoes contrast reversal for one wall propagation direction and retains its original contrast for the opposite direction. z-field amplitude 8 Oe, pulse duration 500 ns. From left to right $t=0$, 45, and 100 ns. Field of view: $20\times45\ \mu m^2$.

during a single long pulse. The reason is that the active field is the total field H_z consisting in the external field H_a and the field produced by the gradient times wall displacement. So that for a long enough pulse (e.g., 500 ns) where the wall can attain equilibrium before the pulse ends, opposite VBL contrast behavior (reversal or not) are seen at the leading and trailing edges. To summarize the experimental results, it appears that, for any configuration, one total field will induce reversal and the opposite not. If we restrict to the domain configuration in our gradient system, reversal occurs when the VBL displaces towards negative x in our conventions.

B. Discussion

This nonequivalence is striking. The combined motion of VBL's and HBL's is a complex, 3D problem. Recently 3D dynamic simulations have become feasible on large-scale computers.[21,22] Among the available simulation results, we shall refer to Ref. 23, the work closest to the present situation of an isolated VBL, set into motion for a long length of time.

Let the two wall segments on both sides of the VBL be called head and tail, according to the direction of VBL motion. The gyrotropic force picture[20] indicates that the head HBL comes from the surface where the VBL has a 0π span, whereas the tail HBL uses the opposite surface, where the VBL has a local 2π span. Consequently, the head HBL has the same core magnetization as the VBL, and the tail the opposite one. Figure 17(b) draws the

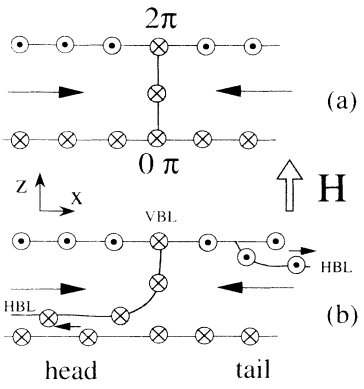

FIG. 17. Schematic interactions between HBL's and a VBL: (a) wall at rest; (b) HBL's are nucleated.

schematic picture which can be derived from the 3D simulation results: The head HBL and the VBL form, in fact, a single line.[23] Motion of the head HBL results in a shortening of the VBL, hence its contrast reduction. Meanwhile, the tail HBL develops at its extremity a vertical segment—a VBL—of charge opposite to the original VBL, therefore of opposite contrast.

If these two VBL's are close enough (typically much less than the size of the microdeformation associated with one VBL, i.e., 2.5 μm for this sample), their contrasts should combine. In that case, the global VBL contrast should reverse each time the HBL's cross the middle of the sample: The global σ charge crosses the zero line at that time. And indeed, in the case showing reversal (e.g., the top of Fig. 16), only two reversals are seen, one at $t\approx50$ ns and the other at $t\approx250$ ns, in agreement with the calculated HBL position (see Fig. 12).

If, however, the two lines were to stay far apart, one should see, instead of a reversal, first a reduction of the original contrast and the apparition in the tail wall segment of an opposite contrast region, followed by a gradual return to the initial situation. To avoid any blurring effect caused by the irregular part of the VBL motion, we recorded snapshots (one video frame, no averaging) of a line in a case where the contrast does not reverse. They are shown in Fig. 18. The contrast of the tail VBL can be seen to build up gradually, but the original VBL does not seem to have a reduced contrast. It seems even to increase.

What determines the distance between the VBL and the outcrop of the tail HBL is not well known. But there seems to be no reason for it to be dependent on the sense of VBL motion. For example, the asymmetry between the two surfaces of the film cannot be invoked, since exchanging the line core magnetization implies the use of the other pulse polarity to have contrast reversal: This exchanges the roles of the surfaces.

C. Dynamic charges mechanism

A tentative explanation may however be proposed. In fact, a VBL moving along the wall is anticipated to distort the latter, much in the same way as does a moving HBL. In the VBL case only a wall lag is expected, be-

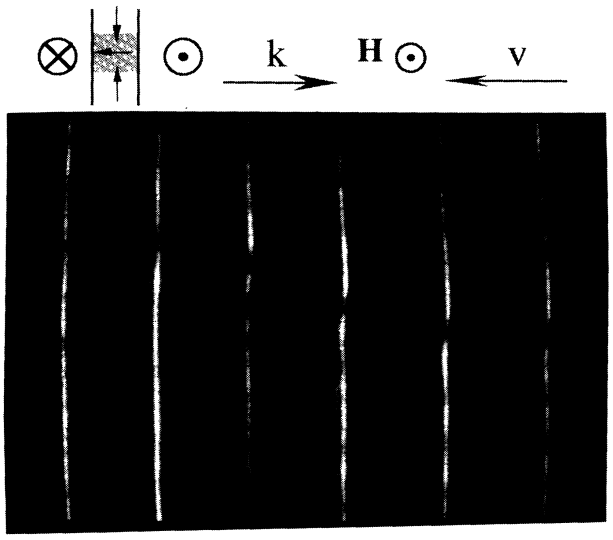

FIG. 18. Snapshots of a VBL submitted to a +8 Oe z-field pulse. From left to right, $t=0$, 50, 100, 150, 200, and 250 ns. The VBL has a core magnetization opposite to that of the dark VBL in Figs. 15 and 16, and experiences an opposite gyrotropic force. Note the shape of the wall distorted region. Each picture is $10\times65\ \mu m^2$.

cause there exists no energy dependence on VBL position forcing it to come back when the total field becomes too low. That lag can be discerned in Figs. 15 and 16, and was mentioned in the introduction. Also, qualitatively identical but much more pronounced lags have been shown by Chetkin *et al.*[24] who proposed a calculation of the shape of the distortion. The shape is asymmetric, with a steep head and an extended tail. Forgetting about the tail, the steep head looks like a kink in the wall at the line position. Inside that kinked wall surface, the VBL is somehow inclined towards the head HBL. Therefore, the kink also should be inclined (Fig. 19). In such a situation, charges occur on the kink, arising from the domain magnetizations. Going into the details, it can be realized that the induced dynamical charge is of sign opposite to the original σ charge when the VBL moves towards negative x, and of the same sign for positive x displacement. Consequently, such a mechanism reproduces the experimental asymmetry. In order to go a step further and gain a decisive understanding of the observed phenomena, 3D dynamical simulations inbedding a single vertical line in a wall section which is long enough to display the wall tilt, seem highly necessary.

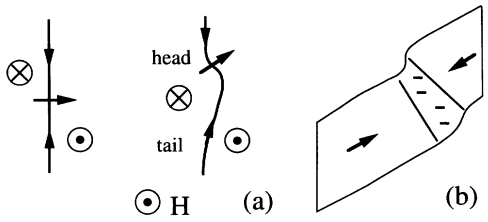

FIG. 19. Schematic "dynamic" wall distortion at VBL location: (a) a kink forms (top view); (b) assumed resultant dynamic wall distortion and associated charges. To those "dynamic" charges should be added the "static" σ charges inherent to VBL's.

V. CONCLUSION

Anisotropic-dark-field optical imaging has allowed for a quantitative, time-resolved monitoring of the wall tilt in bubble garnets during a pulsed-field experiment. The wall tilt can be directly correlated with the position of a horizontal Bloch line within the wall. A very good agreement is obtained between experimental wall diffracted intensity versus time data, and the results of a solution of Slonczewski's equations for a wall of variable shape.

Therefore, a new dimension of wall dynamics, namely its transient shape, becomes accessible to experiment, though in an indirect way. That shape is much more sensitive to wall internal processes than the thickness averaged displacement, which was the experimental touchstone to the experiments that led to the establishment of the wall and lines dynamic theory.

In order to understand the new information available, more theoretical results are necessary, either from a Slonczewski-type approach or from *ab initio* calculations. We propose that the diffracted intensity should be systematically evaluated, as a data processing tool, when simulating wall internal processes. A simple formula for this calculation was proposed and tested by us before.

More generally, the measurement of wall diffracted intensities might prove possible in samples having a high enough Faraday rotation, but where the static wall microdeformation at a VBL is too small to be observed. In that way, HBL processes could become directly measurable in these materials.

ACKNOWLEDGMENTS

It is our pleasure to thank J. Ben Youssef, O. Navarro, J. M. Desvignes, and H. Le Gall at Laboratoire de Magnétisme et Matériaux Magnétiques, CNRS Meudon, for the growth of the sample (TP 010) and acknowledge fruitful discussions with L. Zimmermann from SAGEM.

*On leave from the Institute of Physics, Academy of Sciences, Na Slovance 2, 180 40 Prague 8, Czech Republic.

[1]A. P. Malozemoff and J. C. Slonczewski, *Magnetic Domain Walls in Bubble Materials* (Academic, New York, 1979).

[2]S. Konishi, IEEE Trans. Magn. **MAG-19**, 1838 (1983).

[3]P. J. Grundy, D. C. Hothersall, G. A. Jones, B. K. Middleton, and R. S. Tebble, Phys. Status Solidi A **9**, 79 (1972).

[4]T. M. Morris, G. J. Zimmer, and F. B. Humphrey, J. Appl. Phys. **47**, 721 (1976). Global wall mobility measurements had before shown the dynamic influence of VBL's: See, G. P. Vel-

la Colerio, A. Rosencwaig, and W. J. Tabor, Phys. Rev. Lett. **29**, 949 (1972); and A. P. Malozemoff and J. C. Slonczewski, *ibid.* **29**, 952 (1972).
[5]S. Konishi, K. Matsuyama, and K. Narita, Jpn. J. Appl. Phys. **18**, 1855 (1979).
[6]T. Suzuki *et al.*, IEEE Trans. Magn. **MAG-22**, 784 (1986).
[7]A. Thiaville, J. Ben Youssef, Y. Nakatani, and J. Miltat, J. Appl. Phys. **69**, 6090 (1991).
[8]T. J. Gallagher and F. B. Humphrey, J. Appl. Phys. **50**, 7093 (1979).
[9]A. Thiaville, K. Patek, and J. Miltat (unpublished).
[10]A. S. Logginov and A. V. Nicolaev (private communication); A. S. Logginov, A. V. Nikolaev, and V. V. Dobrovitski, IEEE Trans. Magn. **29**, 2590 (1993).
[11]A. Thiaville and J. Miltat, J. Appl. Phys. **68**, 2883 (1990).
[12]A. Thiaville and K. Patek, J. Magn. Magn. Mater. **124**, 355 (1993).
[13]F. B. Humphrey, IEEE Trans. Magn. **MAG-11**, 1679 (1975).
[14]A. Thiaville and J. Miltat (unpublished).
[15]J. Ben Youssef, A. Thiaville, O. Navarro, J. M. Desvignes, and H. Le Gall, IEEE Trans. Magn. **27**, 5505 (1991).
[16]B. E. Argyle, J. Slonczewski, and A. E. Mayades, *Magnetism and Magnetic Materials 1971,* Proceedings of the 17th Annual Conference on Magnetism and Magnetic Materials, edited by D. C. Graham and J. J. Rhyne, AIP Conf. Proc. No. 5 (AIP, New York, 1971), p. 175.
[17]J. C. Slonczeswki, Int. J. Magn. **2**, 85 (1972).
[18]B. E. MacNeal and F. B. Humphrey, IEEE Trans. Magn. **MAG-15**, 1272 (1979).
[19]J. Miltat, V. Laska, A. Thiaville, and F. Boileau, J. Phys. (Paris) **49**, C8-1871 (1988).
[20]A. A. Thiele, Phys. Rev. Lett. **30**, 230 (1973).
[21]Y. Nakatani and N. Hayashi (unpublished).
[22]A. Bagnérés, G. N. Patterson, and F. B. Humphrey, IEEE Trans. Magn. **27**, 5501 (1991).
[23]A. Bagnérés and F. B. Humphrey, IEEE Trans. Magn. **28**, 2344 (1992).
[24]M. V. Chetkin *et al.*, Zh. Eksp. Teor. Fiz. **94**(11), 164 (1988) [Sov. Phys. JETP **67**, 2269 (1988)].

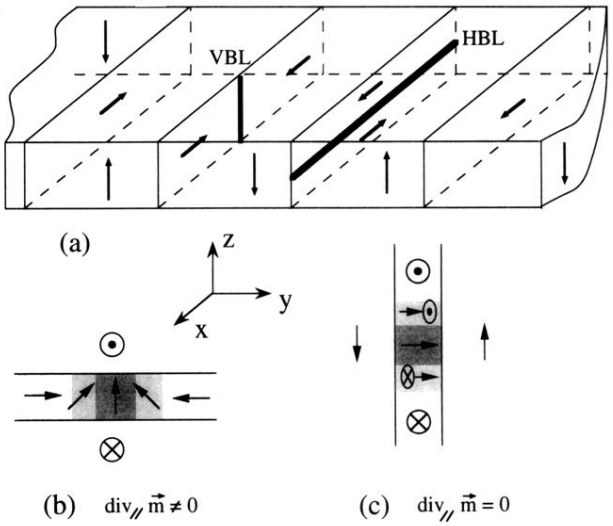

FIG. 1. (a) General drawing of domains, walls (shaded) and lines in a bubble garnet film, in which the easy axis is perpendicular to the film plane. The coordinate system used throughout the paper is figured, with z the easy axis, y the wall normal, and x along the wall. The magnetization distributions characteristic of a vertical Bloch line (VBL) and a horizontal Bloch line (HBL) are shown in (b) (view along z axis) and (c) (view along x axis), respectively. The magnetization direction $\mathbf{m}$ is symbolized by arrows when in the drawing plane and by dot (resp. cross) when perpendicular to that plane, pointing toward (resp. away from) the observer.

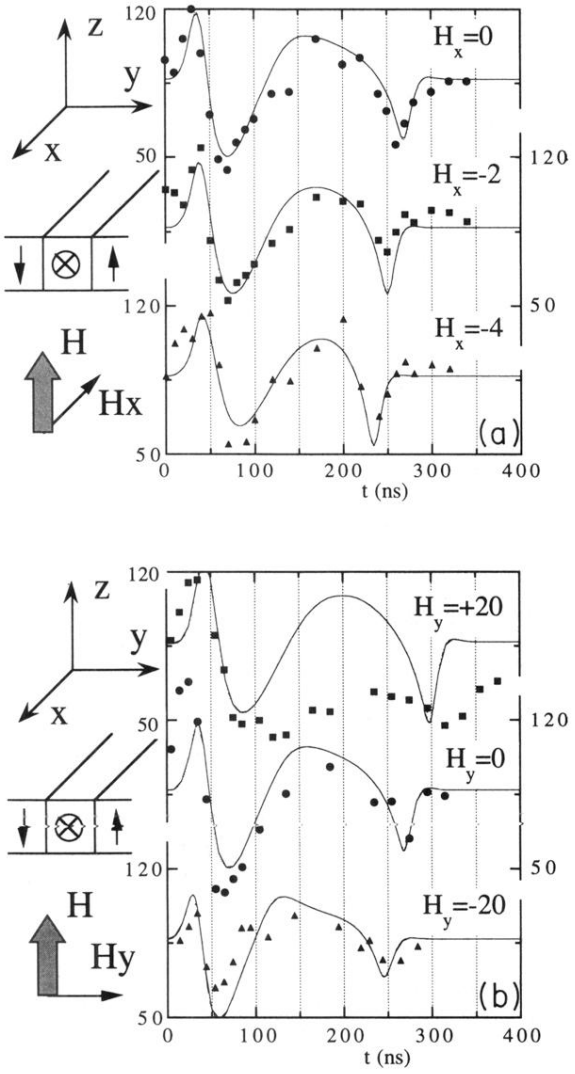

FIG. 14. In conditions identical to those of Fig. 12, influence of a static in plane field (a) parallel to the wall and along its magnetization; (b) perpendicular to the wall. Points are measurement, curves calculation. Field values are indicated in Oe. The +20 Oe values seem to suffer from an experimental artifact but still show the time shift of the salient features.

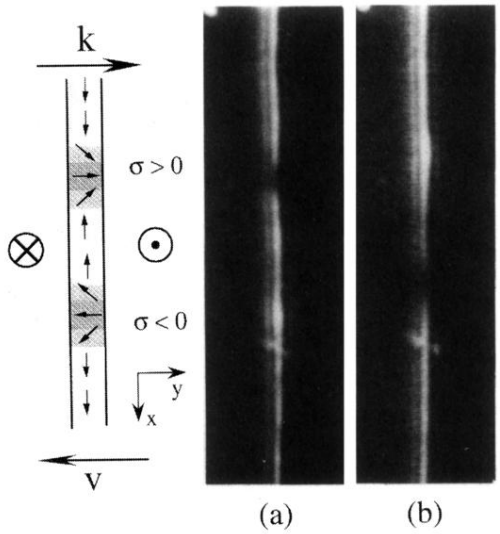

FIG. 15. A pair of winding VBL's: (a) at rest; (b) after 75 ns of a 8.8 Oe, 500 ns z-field pulse. Note the parallel displacement of both lines towards the top of the pictures and their contrast reversal between $t=0$ and $t=75$ ns. Field of view: $25\times85\ \mu m^2$.

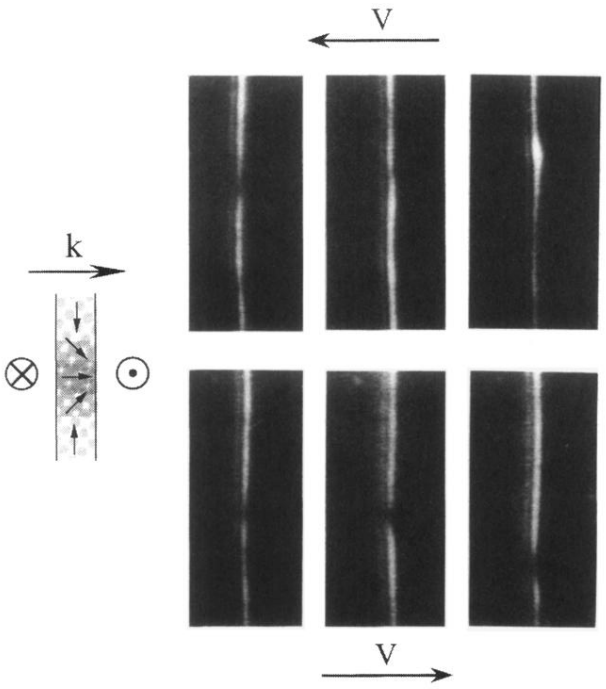

FIG. 16. Difference in dynamic VBL contrast behavior upon reversing the wall velocity: The same line undergoes contrast reversal for one wall propagation direction and retains its original contrast for the opposite direction. z-field amplitude 8 Oe, pulse duration 500 ns. From left to right $t=0$, 45, and 100 ns. Field of view: $20\times45\ \mu m^2$.

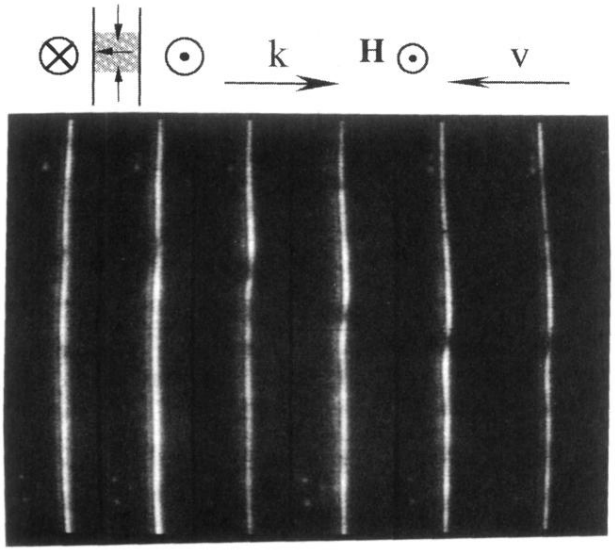

FIG. 18. Snapshots of a VBL submitted to a +8 Oe z-field pulse. From left to right, $t=0$, 50, 100, 150, 200, and 250 ns. The VBL has a core magnetization opposite to that of the dark VBL in Figs. 15 and 16, and experiences an opposite gyrotropic force. Note the shape of the wall distorted region. Each picture is $10\times65\ \mu m^2$.

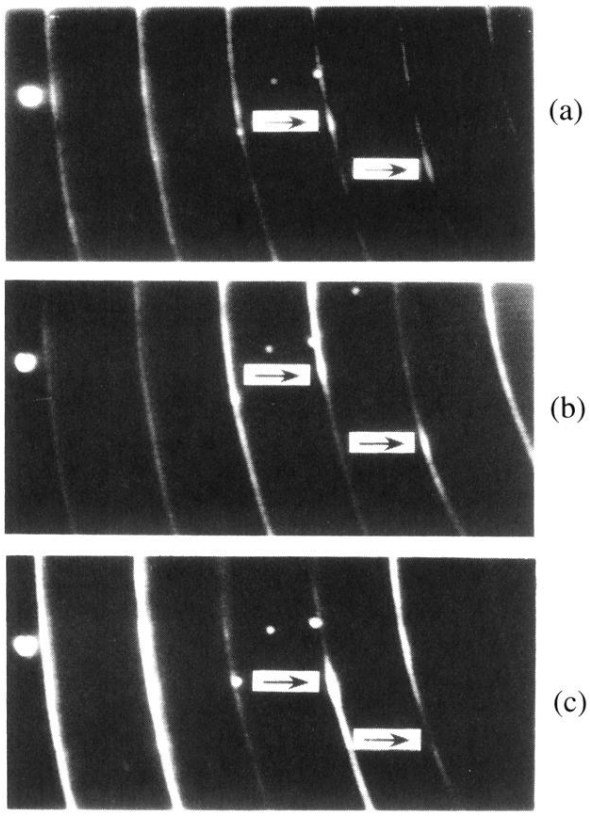

FIG. 2. Effect of a 10 Oe, 500 ns duration z-field pulse on the sample, as revealed by anisotropic-dark-field observation. (a) Wall picture at rest. Arrows indicate the location of VBL's. The other pictures are taken at a time t after pulse onset, with $t=35$ ns for (b) and $t=60$ ns for (c). Field of view: $65\times30\ \mu m^2$.

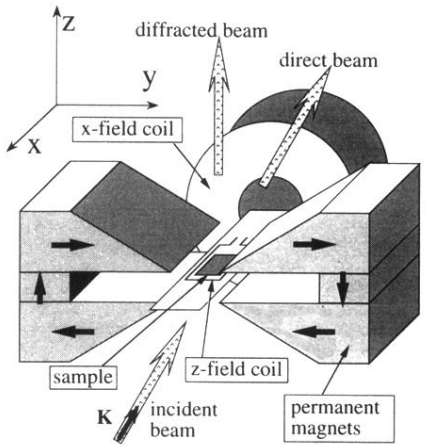

FIG. 3. *Z*-field gradient setup with drive coils. The incident, direct and diffracted optical beams are also drawn. **K** is the wave vector of the incident light, **k** its projection onto the sample plane, and lies along the *y* axis.

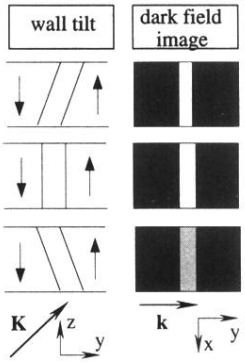

FIG. 4. Schematic relation between wall tilt and contrast under anisotropic-dark-field illumination.

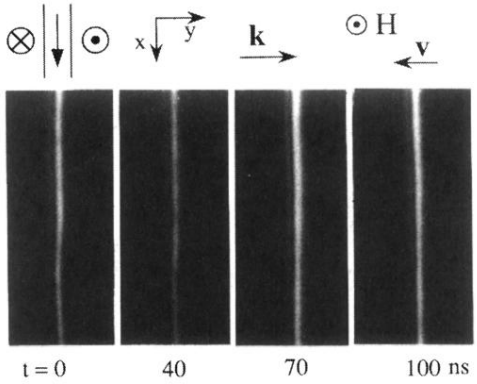

FIG. 5. Wall diffracted intensity as a function of time under the action of a 8 Oe, 500 ns duration z-field pulse. Field of view: $20 \times 45\ \mu m^2$. The drawings refer to the experimental conditions.

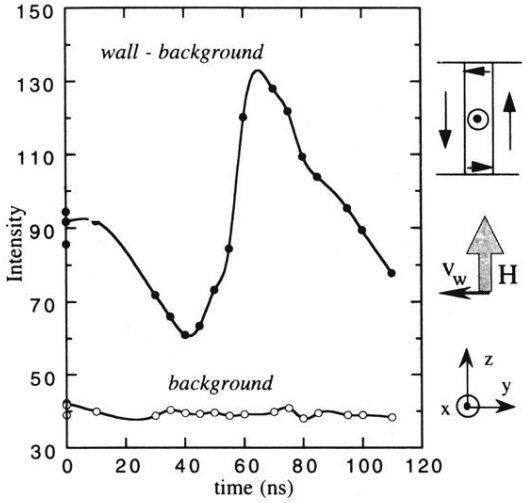

FIG. 7. Background level and diffracted intensity minus background vs time (first 100 ns) recorded for a wall with a $M_x > 0$ Bloch magnetization component. Z-field pulse amplitude 8 Oe, duration 500 ns. The curves serve as a guide to the eye.

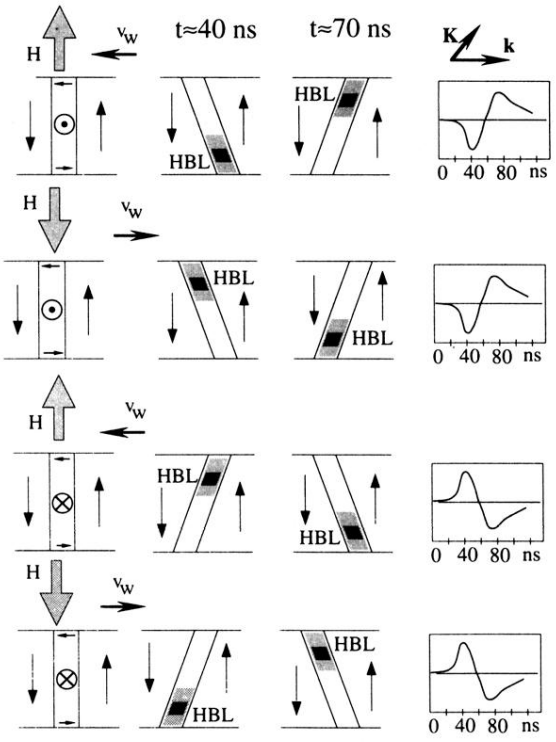

FIG. 9. Schematic time-resolved correlations between wall tilt and HBL location as a function of wall translation direction and Bloch magnetization component. The columns refer, from left to right, to the experimental conditions, the expected HBL motion with associated tilts, and the schematic experimental time evolution of wall contrast.